communications physics

Article

https://doi.org/10.1038/s42005-024-01564-2

Collective non-Hermitian skin effect: point-gap topology and the doublon-holon excitations in non-reciprocal many-body systems

Check for updates

Beom Hyun Kim [1], Jae-Ho Han[1] & Moon Jip Park[2]

Open quantum systems provide a plethora of exotic topological phases of matter that have no Hermitian counterpart. Non-Hermitian skin effect, macroscopic collapse of bulk states to the boundary, has been extensively studied in various experimental platforms. However, it remains an open question whether such topological phases persist in the presence of many-body interactions. Previous studies have shown that the Pauli exclusion principle suppresses the skin effect. In this study, we present a counterexample by demonstrating the presence of the skin effect in doublon-holon excitations. While the ground state of the spin-half Hatano-Nelson model shows no skin effect, the doublon-holon pairs, as its collective excitations, display the many-body skin effect even in strong coupling limit. We establish the robustness of this effect by revealing a bulk-boundary correspondence mediated by the point gap topology within the many-body energy spectrum. Our findings underscore the existence of non-Hermitian topological phases in collective excitations of many-body interacting systems.

Dissipation is a ubiquitously observed phenomenon in many physical systems. In quantum systems, the presence of the dissipation leads to complex-valued eigenenergies, which mark the onset of non-Hermitian quantum mechanics. Non-reciprocal interactions, which are typical in out-of-equilibrium phenomena, are another important source of non-Hermiticity. The broad applicability of non-Hermitian quantum mechanics has attracted considerable interest in various fields of physics, such as high-energy physics[1–4], optics[5–10], cold atoms[11–15], and condensed matter systems[16–23].

Recent progress in the field of non-Hermitian topological phases has shown great promise in discovering new types of topological phases[24–36]. The non-Hermitian skin effect (NHSE), which exhibits the macroscopic collapse of the eigenstates to the boundary, is the representative example[37–52]. However, the fate of the NHSE in the presence of the many-body interaction is still elusive. Previous studies reveal that the NHSE can be fragile against many-body effects[53–58]. For instance, in the half-filled interacting Hatano-Nelson model, the macroscopic accumulation of charge at the boundary is generally prohibited by the Pauli exclusion principle.

In this work, we firstly establish the case that the NHSE robustly exists as a form of collective excitations. Unlike spinless models, the antiferromagnetic Mott insulator ground states of the spin-half Hatano-Nelson model harbor the doublon-holon pairs as well-defined collective excitations even in strong interacting limits. Here, we define the state which shows the minimum value of the real part of complex energies as the ground state because the imaginary part of energies is regarded as the dissipation character of non-Hermitian states. While the ground state does not exhibit the NHSE, we show that the excited states with the doublon-holon pairs show the helical skin effect, where the doublon and the holon exhibit the counterpropagating accumulations of the charge at the opposite boundaries. We formally establish this exotic collective NHSE by illustrating bulk-boundary correspondence mediated by point-gap topology in the many-body energy spectra.

Results and discussion

Lattice model and symmetries

We consider the one-dimensional interacting Hatano-Nelson model of spin-half fermions, which is described by the following Hamiltonian:

$$H = -t\sum_{l=0}^{L-2}\sum_{\sigma}\left(e^{A}c_{l+1,\sigma}^{\dagger}c_{l,\sigma} + e^{-A}c_{l,\sigma}^{\dagger}c_{l+1,\sigma}\right) + U\sum_{l=0}^{L-1} n_{l,\uparrow}n_{l,\downarrow} + H_B. \quad (1)$$

[1]Center for Theoretical Physics of Complex Systems, Institute for Basic Science, Daejeon 34126, Republic of Korea. [2]Department of Physics, Hanyang University, Seoul 04763, Republic of Korea. e-mail: moonjippark@hanyang.ac.kr

Here, $c^{\dagger}_{l,\sigma}$ ($c_{l,\sigma}$) are the fermion creation (annihilation) operators with spin σ ($=\uparrow,\downarrow$) at the l-th site, $n_{l,\sigma}=c^{\dagger}_{l,\sigma}c_{l,\sigma}$ is the number operator, and U is the strength of on-site Coulomb repulsion between doubly occupied fermions. The lattice size is denoted by L and A represents the imaginary vector potential that introduces non-reciprocal hopping[16,17]. The boundary term H_B accounts for the hopping Hamiltonian between the end sites. For example, in open boundary conditions (OBC), H_B is 0, while $H_B=-t(e^{A}c^{\dagger}_{0,\sigma}c_{L-1,\sigma}+e^{-A}c^{\dagger}_{L-1,\sigma}c_{0,\sigma})$ for periodic boundary conditions (PBC). In general twisted boundary conditions (TBC), H_B takes a form, $-t(e^{A+i\phi}c^{\dagger}_{0,\sigma}c_{L-1,\sigma}+e^{-A-i\phi}c^{\dagger}_{L-1,\sigma}c_{0,\sigma})$, where ϕ represents the $U(1)$-gauge (magnetic) flux.

The symmetry of the Hamiltonian depends on both boundary conditions and the presence of the many-body interactions. In the non-interacting limit ($U=0$), under PBC and TBC the Hamiltonian operator is normal ($HH^{\dagger}=H^{\dagger}H$), which allows to have orthonormalized eigenstates (see Supplementary Note 1). The corresponding eigenvalue spectra in PBC can form a closed contour with non-trivial point gap topology. In the corresponding OBC, the normality is lost. Instead, there exists the similarity transformation with the invertible operation S that satisfies $H_{A=0}=S^{-1}HS$, where $H_{A=0}$ is the Hermitian Hamiltonian without the imaginary vector potential A (see Supplementary Note 2). As a result, all eigenvalues exhibit purely real numbers[59].

Even in the finite many-body interaction ($U\neq 0$), we can find the similarity transformation S such that $H_{A=0}=S^{-1}HS$ under OBC, resulting the purely real eigenvalues. However, the normality is broken regardless of the boundary condition due to the inclusion of U. Moreover, H for PBC and TBC becomes $\mathcal{PT}$-pseudo-Hermitian, where $\mathcal{P}$ and $\mathcal{T}$ are inversion and time-reversal operators, respectively (see Supplementary Note 3). Consequently, the eigenvalues are either real or occur in complex-conjugate pairs[60].

Non-Hermitian skin effect

We represent the many-body eigenstates using orthonormal basis states:

$$|\Psi_n\rangle=\prod_{j=1}^{N}c^{\dagger}_{l_{nj},\sigma_{nj}}|vac\rangle, \tag{2}$$

where l_{nj} and σ_{nj} denote the site index and spin state of the jth fermion for the nth basis state, respectively. $|vac\rangle$ represents the vacuum state, and N is the total number of fermions. The similarity transformation S such that $H_{A=0}=S^{-1}HS$ under OBC is given as following (see Supplementary Note 2):

$$S=\sum_{n}e^{A\sum_{j=1}^{N}l_{nj}}|\Psi_n\rangle\langle\Psi_n|. \tag{3}$$

The non-orthonormal factor $C_n(A)=e^{A\sum_{j=1}^{N}l_{nj}}$ causes coefficients of eigenstates to vary exponentially with A, playing a crucial role in determining the NHSE in many-body systems[56,61].

With respect to the half-filled ground state ($N=L$), $C_n(A)$ can vary depending on the distribution of doubly occupied sites, called doublons, and empty sites, referred to as holons (see Supplementary Note 4). Explicitly, let N_d be the total number of doublon-holon pairs. $C_n(A)$ is expressed as

$$C_n(A)=e^{A\frac{L(L-1)}{2}}e^{A\sum_{j=1}^{N_d}\left(l^{d}_{nj}-l^{h}_{nj}\right)}, \tag{4}$$

where l^{d}_{nj} and l^{h}_{nj} denote the site indices of the jth doublon and holon for the nth basis state $|\Psi_n\rangle$, respectively. For states with no doublon-holon pair ($N_d=0$), $C_n(A)$ reaches its minimum with a constant value of $e^{A\frac{L(L-1)}{2}}$. These states exhibit little influence from the NHSE. On the other hand, for states with finite doublon-holon pairs, $C_n(A)$ grows exponentially as the strength of A increases. The larger the segregation between doublons and holons, quantified by $\sum_{j=1}^{N_d}(l^{d}_{nj}-l^{h}_{nj})$, the larger $C_n(A)$ becomes. Hence, the NHSE in the half-filled case is characterized by the segregation of doublons and holes.

The relation between the NHSE and the segregation of doublons and holons can be explained by considering the non-reciprocal mobility of these particles. As illustrated in Fig. 1, let us imagine that a doublon-holon pair forms between neighboring sites in a half-filled state. When a positive $A>0$ is present, the hopping strength from the left site to the right site becomes larger than the opposite direction. This enhances the fermion on the left side of the holon site to preferentially occupy that site, leading to the holon's movement to the right. In contrast, one of the fermions occupying the doublon site is more likely to hop to the next site on the right, resulting in the doublon's movement to the left. As a result, doublons and holons become separated and localized at opposite boundary sites under OBC. Conversely, for PBC, doublons and holons merge again. This distinctive non-reciprocal behavior of doublons and holons underpins the emergence of the NHSE in the half-filled case.

In many-body systems governed by the Pauli exclusion principle, one effective approach to demonstrate the NHSE is by quantifying the asymmetry in the distribution of number density along an open-boundary chain[56]. To achieve this, we calculate the number density distribution of the right eigenstates using the formula: $n^{R}_{E}(l)=\langle\Psi^{R}_{E}|\sum_{\sigma}c^{\dagger}_{l,\sigma}c_{l,\sigma}|\Psi^{R}_{E}\rangle/\langle\Psi^{R}_{E}|\Psi^{R}_{E}\rangle$. This distribution's asymmetry results in the number imbalance of fermions located at below $L/2$ ($0\le l<L/2$) and above $L/2$ ($L/2\le l<L$) sites. We can quantify this imbalance with the following formula:

$$\mathcal{I}^{R}_{E}=\sum_{L/2\le l<L}n^{R}_{E}(l)-\sum_{0\le l<L/2}n^{R}_{E}(l). \tag{5}$$

The occurrence of non-zero values for $\mathcal{I}^{R}_{E}$ is a distinctive indicator of the many-body NHSE, as detected within right eigenstates.

Figure 2 exhibits the calculated number density distribution, clearly showing that the asymmetric nature is present under OBC for both non-interacting ($U=0$) and interacting ($U\neq 0$) cases. The corresponding finite values of imbalance $\mathcal{I}^{R}_{E}$ affirm this. However, the situation differs for PBC, where $\mathcal{I}^{R}_{E}$ consistently equals zero. These results depict the NHSE in non-reciprocal many-body systems.

In the non-interacting case ($U=0$), $\mathcal{I}^{R}_{E}$ exhibits an arch-like pattern, ranging from about 1 to roughly 7 for $L=8$ as shown in Fig. 2a. In contrast, strong interactions ($U=10t$) yield a stair-like $\mathcal{I}^{R}_{E}$ pattern. This can be understood by the spectral properties of the Mott insulating region. With a substantial Coulomb repulsion (U), eigenvalues mainly depend on U strength, leading to sizable separations related to the number of doublon-holon pairs (N_d). When N_d-dominated states prevail in the eigenstates, $\mathcal{I}^{R}_{E}$ attains a maximum value of around $2N_d$ for OBC. This feature is well captured by Fig. 2b.

Furthermore, the non-reciprocal hopping causes opposing doublon and holon propagation. Initially, they gather at opposing boundaries for finite A. The Pauli exclusion principle then drives further accumulation near by initial sites. This pattern is visually evident in the calculated number density distributions, depicted in Fig. 2c–f (see also Supplementary Fig. 2 for the non-interacting case). Consequently, we deduce that the NHSE in the many-body system can be understood through the segregation of doublons and holons within the half-filled Hatano-Nelson model of spin-half fermions.

Complex eigenspectrum and point-gap topology

As shown in Fig. 3a, for PBC, the eigenvalues of the Hamiltonian can take either on purely real values or form complex conjugate pairs. This originates from the pseudo-Hermiticity of the Hamiltonian. To gain a deeper understanding of the spectral properties, we analyze how eigenvalues change with the gauge flux ϕ under TBC. Figure 3b, c provides the trajectory of complex eigenvalues when the real part of the eigenvalue lies between $4t$ and $14t$ (one doublon-holon sector) and between $39t$ and $43t$ (four doublon-holon sector), respectively.

As ϕ changes from 0 to 2π, complex eigenvalues undergo rotations in the complex plane, effectively tracing closed paths alongside other eigenvalues. This rotation ultimately results in non-zero integer winding

numbers, which can be calculated using the formula:

$$W\left(E_p\right) = \oint_0^{2\pi} \frac{d\phi}{2\pi i} \frac{d}{d\phi} \log \det\left[H(\phi) - E_p\right]. \tag{6}$$

Here, E_p stands for the point gap of the complex energy[54,55]. This behavior highlights the intriguing topological aspects inherent to the system.

In the non-interacting case, all complex eigenvalues wind around the origin ($E = 0$). It implies that the point gap is straightforwardly identified at the center of the complex plane (see Supplementary Fig. 3). However, in the interacting case, as seen in Fig. 3b and c, multiple point gaps are not isolated but emerge near the energy center of doublon-holon sectors. This multiplicity of point gaps defines the non-Hermitian topology of non-reciprocal many-body systems.

In the strong interaction limit, the many-body NHSE does not emerge for eigenstates mainly contributed to states with no doublon-holon pair in the half-filled case. Correspondently, eigenvalues below zero remain purely real even for PBC. In the second-order perturbation limit, the effective Hamiltonian in no doublon-holon sector is described with the Heisenberg interaction, given as $H_{\text{eff}} = J\sum_l \mathbf{S}_l \cdot \mathbf{S}_{l+1}$[62], in the strong interaction limit (see Supplementary Note 5).

When the total number of doublon-holon pairs is $L/2$, $L/2$ number of doublons and holons occupy all lattice sites. In this situation, we can construct the effective model using attractive half-filled hard-core bosons with non-reciprocal hopping in the second-order perturbation limit. The effective attractive interaction, hopping strength, and imaginary vector potential are estimated by $U_{\text{eff}} = -\frac{4t^2}{U}$, $t_{\text{eff}} = \frac{2t^2}{U}$, and $A_{\text{eff}} = 2A$, respectively (see Supplementary Note 5). Since $|U_{\text{eff}}|/t_{\text{eff}} = 2$ is much smaller than U/t and A_{eff} is the twice of A, the robustness of complex eigenvalues can be maintained even when U exceeds t much largely.

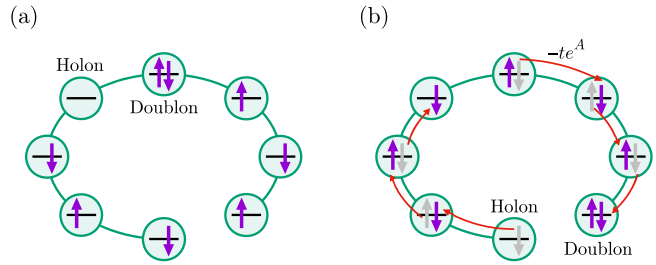

Fig. 1 | The skin effect of doublon-holon excitations. Schematic diagrams of (**a**) doublon (doubly occupied site) and holon (empty site) excitations, and (**b**) their motion in the presence of non-reciprocal hopping. As illustrated in **b**, non-reciprocal hopping, denoted by red arrows, results in the rightward (leftward) movement of doublons (holons). The gray arrows in **b** represent the initial positions of fermion spins prior to hopping. Under open boundary conditions, doublon and holon become localized at opposite edges of one dimensional chain. This segregation in localized doublon and holon is responsible for the Non-Hermitan skin effect.

Topological transition and exceptional points

Due to the Hermitian nature of the Coulomb interaction part in Eq. (1), all eigenvalues asymptotically converge to real numbers in the U-infinite limit even for PBC. All complex conjugate eigenpairs in finite U eventually transform into two real eigenvalues. This transition involves the gradual separation of two real eigenvalues, following the merging of complex conjugate eigenpairs along the real axis. This spectral behavior resembles the $\mathcal{PT}$-phase transition[63,64]. Figure 4a, b well depict the sequential occurrences of these transitions when U gradually increases.

We further examine the evolution of complex eigenvalues in the presence of the gauge flux ϕ under TBC. As shown in Fig. 4c–f, complex conjugate eigenpair are connected by the ϕ evolution before the transition, while that eigenpair get separated after the transition. It implies the winding number in Eq. (6) changes undergoing the transition, giving the different point-gap topology[56,63]. Moreover, two eigenstates of the eigenpair involved in the transition collapse into a singular state at the transition point (see Supplementary Note 6). The transition point of the winding number is identified as $\mathcal{PT}$-like topological transitions accompanying the exceptional point (see Supplementary Note 7 for the topological transitions as a function of A).

Beyond half-filling

When the fermion filling deviates from half-filling, unpaired doublons or holons emerge. Consequently, the NHSE is not exclusively determined by the doublon-holon pairs. Unpaired holons or doublons can also contribute to its manifestation.

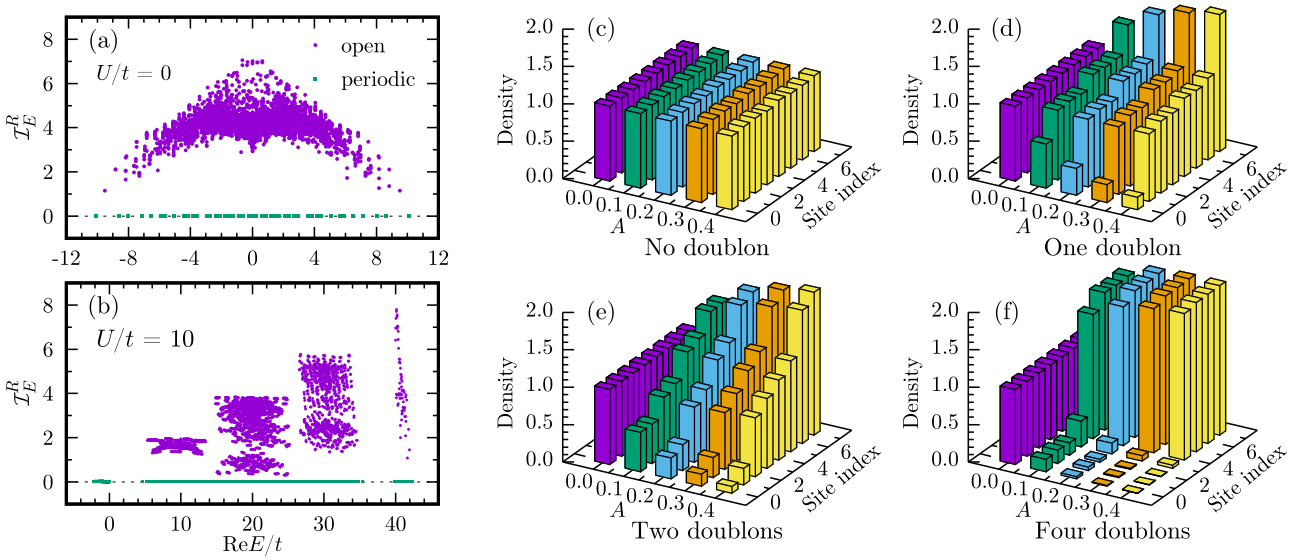

Fig. 2 | The number density imbalance under open boundary conditions. The number density imbalance in the half-filled Hatano-Nelson model of spin-half fermions under both open boundary conditions (OBC) and periodic boundary conditions when the ratio of Coulomb repulsion U to hopping strength t (U/t) is (**a**) 0 and (**b**) 10, and the imaginary vector potential A is 0.3. The imbalance $\mathcal{I}_E^R$ is calculated by $\sum_{L/2\le l<L} n_E^R(l) - \sum_{0\le l<L/2} n_E^R(l)$, where $n_E^R(l)$ is the number density of right eigenvalues at the lth site. **c**–**f** the number density distributions as a function of imaginary gauge potential A for specific right eigenstates, where no, one, two, and four doublon-holon pairs play a dominant role for OBC. All results are obtained for a lattice size of eight ($L = 8$).

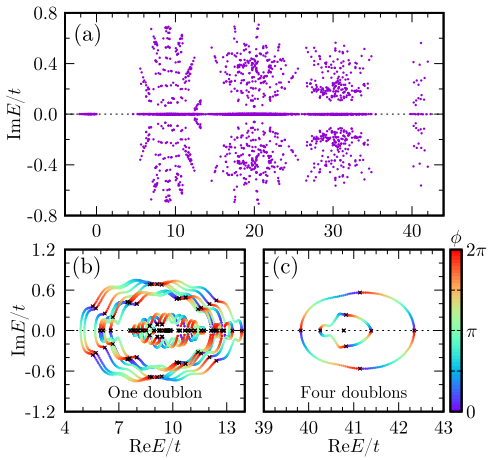

Fig. 3 | Complex eigenspectrum under periodic boundary conditions. **a** Eigenvalue spectrum in the half-filled Hatano-Nelson model of spin-half fermions when the ratio of Coulomb repulsion U to hopping strength t (U/t) is 10 and the imaginary vector potential A is 0.3. Notably, even under strong interaction limit, complex eigenvalues remain robust within finite doublon-holon sectors. Spectral evolution of eigenvalues as functions of the gauge flux ϕ for twisted boundary conditions in **b** one and **c** four doublon-holon sectors. For simplicity, only eigenvalues corresponding to the crystal momentum $k = 0$ and the z-component of the total spin $S_z = 0$ are presented in **b** and **c** by utilizing the translation symmetry and S_z conservation (see Methods). Cross points indicate eigenvalues at $\phi = 0$. These spectral data effectively depict the point-gap topology of complex eigenvalues. All results are obtained for a lattice size of eight ($L = 8$).

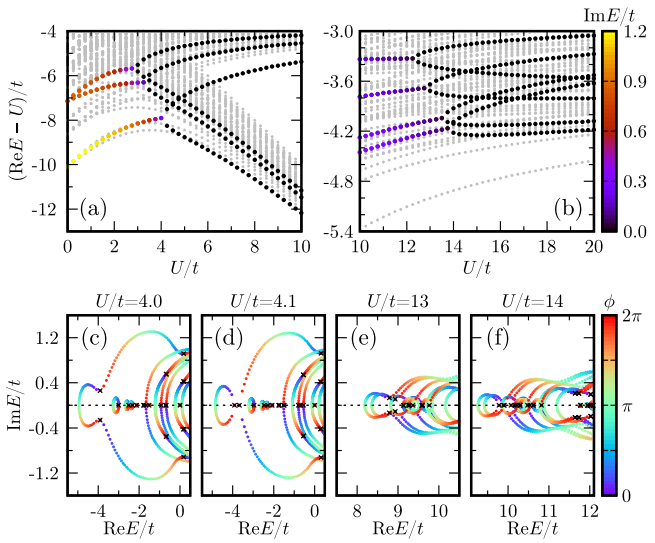

Fig. 4 | Topological transition and exceptional points. Real components of eigenvalues varying with the ratio of Coulomb repulsion U to hopping strength t for (**a**) $0 \le U/t \le 10$ and (**b**) $10 \le U/t \le 20$. **a** and **b** represent the eigenvalue spectrum for no and one doublon-holon sector, respectively. We highlight a few eigenpairs, which perform the transition from complex conjugate pair to two pure real numbers, using color map. **c**–**f** show the spectral evolutions of eigenvalues for the crystal momentum $k = 0$ and the z-component of the total spin $S_z = 0$ eigenstates as a function of the gauge flux ϕ under twisted boundary conditions. All results are obtained when the imaginary vector potential A is 0.3 and the lattice size L is 8.

Let us consider the case in which total number of fermions N is one smaller than the lattice size L. In strong coupling limit, the ground state is primarily determined within the subspace where one holon emerges and the remained sites are singly occupied. Although the effective Hamiltonian between one-fermion sites is described with the magnetic interaction

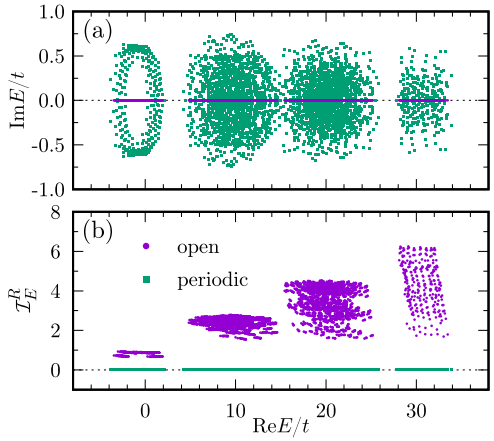

Fig. 5 | Egienspectrum and number density imbalance beyond half-filling. **a** Eigenvalue spectrum and (**b**) the number density imbalance in the Hatano-Nelson model of spin-half fermions under both open and periodic boundary conditions when total number of fermions $N = 7$ is one smaller than the lattice size $L = 8$. The green squares and purple circles refer to the results for periodic and open boundary conditions, respectively. The imbalance $\mathcal{I}_E^R$ is calculated by Eq. (5). All results are obtained when the ratio of Coulomb repulsion U to hopping strength t (U/t) is 10 and the imaginary vector potential A is 0.3.

J which does not induce a non-reciprocal effect, the non-reciprocal hopping leads to the asymmetric movement of an unpaired holon. This results in a complex eigenspectrum even within ground manifolds under PBC. The accumulation of a hole at specific boundary gives rise to an imbalance in the number density under OBC as shown in Fig. 5.

In excited manifolds, both doublon-holon pairs and unpaired holons mutually contribute to the generation of complex eigenvalues and the imbalance in number density under OBC. This interplay is evident in the step-like imbalance profile. The maximum imbalance values of 1, 3, 5, and 7 can be interpreted as the accumulation of unpaired hole plus the segregated doublon-holon pairs. Consequently, the interplay of doublon-holon pairs and unpaired doublons or holons highlights the intricate nature of the NHSE beyond half-filling.

Conclusions

We investigate the intriguing behavior of the many-body NHSE and unique features of eigenspectra in the half-filled interacting Hatano-Nelson model of spin-half fermions. We discover that strong interactions suppress doublon-holon excitations in the ground state, leading to the absence of the NHSE. However, excited eigenstates still exhibit these excitations, driven by non-reciprocal hopping, which causes doublons and holons to move in opposite directions. The spatial segregation of doublon-holon pairs serves the hallmark of the many-body skin modes. Moreover, these modes are attributed to the bulk-boundary correspondence mediated by the point gap topology within complex many-body eigenspectrums.

Experimentally, realizing these effects can be challenging, but open quantum systems such as ultracold atoms can be a promising platform. Experiments with bosonic ultracold atoms have already shown skin effects[13]. Because the dynamics of the systems is governed by the Liouvillian master equations, exploring the interplay between many-body effects and Liouvillian skin effects[15,41,65,66] in such systems holds great potential for unveiling novel physical phenomena of non-Hermitan many-body physics.

Methods

Many-body calculation

Let $\hat{N}$ and $\hat{S}_z$ be operators for the total number of fermions and the z-component of the total spin, given as $\hat{N} = \sum_{l=0}^{L-1}(n_{l,\uparrow} + n_{l,\downarrow})$ and $\hat{S}_z = \sum_{l=0}^{L-1}(n_{l,\uparrow} - n_{l,\downarrow})$. The Hamiltonian of Eq. (1) commutes both $\hat{N}$ and $\hat{S}_z$ operators, regardless of the selected A value and boundary condition.

Thus, we can determine the eigenvalues of the Hamiltonian by considering the subspace in which both $\hat{N}$ and $\hat{S}_z$ are constant. We construct the many-body Hamiltonian adopting orthonormal basis states given as Eq. (2).

For TBC, we can perform a unitary transformation of local fermionic operators as follows:

$$c_{l\sigma}^{\dagger} \to \tilde{c}_{l\sigma}^{\dagger} = e^{il\phi/L} c_{l\sigma}^{\dagger}, \quad c_{l\sigma} \to \tilde{c}_{l\sigma} = e^{-il\phi/L} c_{l\sigma}. \tag{7}$$

This transformation allows us to obtain an effective periodic Hamiltonian as follows:

$$\begin{aligned} H = & -t \sum_{l=0}^{L-2} \sum_{\sigma} \left(e^{A+i\phi/L} \tilde{c}_{l+1,\sigma}^{\dagger} \tilde{c}_{l,\sigma} + e^{-A-i\phi/L} \tilde{c}_{l,\sigma}^{\dagger} \tilde{c}_{l+1,\sigma} \right) \\ & + U \sum_{l=0}^{L-1} \tilde{n}_{l,\uparrow} \tilde{n}_{l,\downarrow} + \tilde{H}_B, \end{aligned} \tag{8}$$

where $\tilde{n}_{l,\sigma} = \tilde{c}_{l,\sigma}^{\dagger} \tilde{c}_{l,\sigma}$ and $\tilde{H}_B = -t \sum_{\sigma} \left(e^{A+i\phi/L} \tilde{c}_{0,\sigma}^{\dagger} \tilde{c}_{L-1,\sigma} + e^{-A-i\phi/L} \tilde{c}_{L-1,\sigma}^{\dagger} \tilde{c}_{0,\sigma} \right)$. In TBC, we represent the many-body states using orthonormal basis states $|\Psi_n\rangle = \prod_{j=1}^{N} \tilde{c}_{n_j,\sigma_{n_j}}^{\dagger} |vac\rangle$.

For PBC and TBC, we can take into account L number of translation operators, defined as $T_l c_{l',\sigma}^{\dagger} T_l^{-1} = c_{l'+l \bmod L,\sigma}^{\dagger}$ $(0 \le l, l' < L)$. T_0 corresponds to the identity operator. With the translation symmetry, the many-body states can be characterized with the crystal momentum $k \in \{0, 2\pi/L, \cdots, 2\pi(L-1)/L\}$. The translation-symmetrized basis states can be expressed as follows:

$$|\Psi_n(k)\rangle = \frac{1}{\sqrt{N_{nk}}} \sum_{l=0}^{L-1} e^{-ikl} T_l |\Psi_n\rangle, \tag{9}$$

where N_{nk} is the normalization factor and $|\Psi_n\rangle$ is the representative state for the nth basis state. $T_l|\Psi_n\rangle$ can be obtained as follows:

$$T_l |\Psi_n\rangle = \prod_{j=1}^{N} T_l c_{n_j,\sigma_{n_j}}^{\dagger} T_l^{-1} |vac\rangle = \prod_{j=1}^{N} c_{n_j+l \bmod L,\sigma_{n_j}}^{\dagger} |vac\rangle. \tag{10}$$

By utilizing the translation symmetry and expressing the basis states in terms of crystal momentum under PBC and TBC, we can effectively reduce the Hilbert space, making it more tractable to calculate the eigenvalues and eigenstates of the Hamiltonian.

Data availability

The authors ensure the availability of the data supporting the findings of the current study in both the article and its Supplementary Materials. Additional information can be provided upon request.

Received: 17 October 2023; Accepted: 18 February 2024;
Published online: 02 March 2024

References

1. Bender, C. M. Making sense of non-Hermitian Hamiltonians. *Rep. Prog. Phys.* **70**, 947 (2007).
2. Jones-Smith, K. & Mathur, H. Non-Hermitian quantum Hamiltonians with $\mathcal{PT}$ symmetry. *Phys. Rev. A* **82**, 042101 (2010).
3. Bender, C. M., Cavero-Pelaez, I., Milton, K. A. & Shajesh, K. PT-symmetric quantum electrodynamics. *Phys. Lett. B* **613**, 97–104 (2005).
4. Alexandre, J., Bender, C. M. & Millington, P. Non-Hermitian extension of gauge theories and implications for neutrino physics. *J. High. Energ. Phys.* **2015**, 111 (2015).
5. Feng, L., El-Ganainy, R. & Ge, L. Non-Hermitian photonics based on parity-time symmetry. *Nat. Photonics* **11**, 752–762 (2017).
6. Özdemir, Ş. K., Rotter, S., Nori, F. & Yang, L. Parity-time symmetry and exceptional points in photonics. *Nat. Mater.* **18**, 783–798 (2019).
7. Miri, M.-A. M. & Alù, A. Exceptional points in optics and photonics. *Science* **363**, eaar7709 (2019).
8. Ozawa, T. et al. Topological photonics. *Rev. Mod. Phys.* **91**, 015006 (2019).
9. Longhi, S. Stochastic non-Hermitian skin effect. *Opt. Lett.* **45**, 5250–5253 (2020).
10. Zhu, X. et al. Photonic non-Hermitian skin effect and non-Bloch bulk-boundary correspondence. *Phys. Rev. Res.* **2**, 013280 (2020).
11. Takasu, Y. et al. PT-symmetric non-Hermitian quantum many-body system using ultracold atoms in an optical lattice with controlled dissipation. *Prog. Theor. Exp. Phys.* **2020**, 12A110 (2020).
12. Guo, S., Dong, C., Zhang, F., Hu, J. & Yang, Z. Theoretical prediction of a non-Hermitian skin effect in ultracold-atom systems. *Phys. Rev. A* **106**, L061302 (2022).
13. Liang, Q. et al. Dynamic Signatures of Non-Hermitian Skin Effect and Topology in Ultracold Atoms. *Phys. Rev. Lett.* **129**, 070401 (2022).
14. Zhou, L., Li, H., Yi, W. & Cui, X. Engineering non-Hermitian skin effect with band topology in ultracold gases. *Commun. Phys.* **5**, 252 (2022).
15. Hamanaka, S., Yamamoto, K. & Yoshida, T. Interaction-induced Liouvillian skin effect in a fermionic chain with two-body loss. *arXiv* https://doi.org/10.48550/arXiv.2305.19697 (2023).
16. Hatano, N. & Nelson, D. R. Localization Transitions in Non-Hermitian Quantum Mechanics. *Phys. Rev. Lett.* **77**, 570–573 (1996).
17. Hatano, N. & Nelson, D. R. Non-Hermitian delocalization and eigenfunctions. *Phys. Rev. B* **58**, 8384–8390 (1998).
18. Fukui, T. & Kawakami, N. Breakdown of the Mott insulator: Exact solution of an asymmetric Hubbard model. *Phys. Rev. B* **58**, 16051–16056 (1998).
19. Kozii, V. & Fu, L. Non-Hermitian Topological Theory of Finite-Lifetime Quasiparticles: Prediction of Bulk Fermi Arc Due to Exceptional Point. *arXiv* https://doi.org/10.48550/arXiv.1708.05841 (2017).
20. Yoshida, T., Peters, R. & Kawakami, N. Non-Hermitian perspective of the band structure in heavy-fermion systems. *Phys. Rev. B* **98**, 035141 (2018).
21. Nagai, Y., Qi, Y., Isobe, H., Kozii, V. & Fu, L. DMFT Reveals the Non-Hermitian Topology and Fermi Arcs in Heavy-Fermion Systems. *Phys. Rev. Lett.* **125**, 227204 (2020).
22. Rausch, R., Peters, R. & Yoshida, T. Exceptional points in the one-dimensional Hubbard model. *N. J. Phys.* **23**, 013011 (2021).
23. Ren, Z. et al. Chiral control of quantum states in non-Hermitian spin-orbit-coupled fermions. *Nat. Phys.* **18**, 385–389 (2022).
24. Gong, Z. et al. Topological Phases of Non-Hermitian Systems. *Phys. Rev. X* **8**, 031079 (2018).
25. Yao, S. & Wang, Z. Edge States and Topological Invariants of Non-Hermitian Systems. *Phys. Rev. Lett.* **121**, 086803 (2018).
26. Yao, S., Song, F. & Wang, Z. Non-Hermitian Chern Bands. *Phys. Rev. Lett.* **121**, 136802 (2018).
27. Kawabata, K., Shiozaki, K., Ueda, M. & Sato, M. Symmetry and Topology in Non-Hermitian Physics. *Phys. Rev. X* **9**, 041015 (2019).
28. Song, F., Yao, S. & Wang, Z. Non-Hermitian Topological Invariants in Real Space. *Phys. Rev. Lett.* **123**, 246801 (2019).
29. Yokomizo, K. & Murakami, S. Non-Bloch Band Theory of Non-Hermitian Systems. *Phys. Rev. Lett.* **123**, 066404 (2019).
30. Deng, T.-S. & Yi, W. Non-Bloch topological invariants in a non-Hermitian domain wall system. *Phys. Rev. B* **100**, 035102 (2019).
31. Okuma, N., Kawabata, K., Shiozaki, K. & Sato, M. Topological Origin of Non-Hermitian Skin Effects. *Phys. Rev. Lett.* **124**, 086801 (2020).
32. Borgnia, D. S., Kruchkov, A. J. & Slager, R.-J. Non-Hermitian Boundary Modes and Topology. *Phys. Rev. Lett.* **124**, 056802 (2020).
33. Bergholtz, E. J., Budich, J. C. & Kunst, F. K. Exceptional topology of non-Hermitian systems. *Rev. Mod. Phys.* **93**, 015005 (2021).
34. Ding, K., Fang, C. & Ma, G. Non-Hermitian topology and exceptional-point geometries. *Nat. Rev. Phys.* **4**, 745–760 (2022).
35. Lin, R., Tai, T., Li, L. & Lee, C. H. Topological non-Hermitian skin effect. *Front. Phys.* **18**, 53605 (2023).

36. Kawabata, K., Numasawa, T. & Ryu, S. Entanglement Phase Transition Induced by the Non-Hermitian Skin Effect. *Phys. Rev. X* **13**, 021007 (2023).
37. Lee, C. H. & Thomale, R. Anatomy of skin modes and topology in non-Hermitian systems. *Phys. Rev. B* **99**, 201103 (2019).
38. Jiang, H., Lang, L.-J., Yang, C., Zhu, S.-L. & Chen, S. Interplay of non-Hermitian skin effects and Anderson localization in nonreciprocal quasiperiodic lattices. *Phys. Rev. B* **100**, 054301 (2019).
39. Imura, K.-I. & Takane, Y. Generalized bulk-edge correspondence for non-Hermitian topological systems. *Phys. Rev. B* **100**, 165430 (2019).
40. Zhang, K., Yang, Z. & Fang, C. Correspondence between Winding Numbers and Skin Modes in Non-Hermitian Systems. *Phys. Rev. Lett.* **125**, 126402 (2020).
41. Yang, Z., Zhang, K., Fang, C. & Hu, J. Non-Hermitian Bulk-Boundary Correspondence and Auxiliary Generalized Brillouin Zone Theory. *Phys. Rev. Lett.* **125**, 226402 (2020).
42. Yi, Y. & Yang, Z. Non-Hermitian Skin Modes Induced by On-Site Dissipations and Chiral Tunneling Effect. *Phys. Rev. Lett.* **125**, 186802 (2020).
43. Schomerus, H. Nonreciprocal response theory of non-Hermitian mechanical metamaterials: Response phase transition from the skin effect of zero modes. *Phys. Rev. Res.* **2**, 013058 (2020).
44. Ghaemi-Dizicheh, H. & Schomerus, H. Compatibility of transport effects in non-Hermitian nonreciprocal systems. *Phys. Rev. A* **104**, 023515 (2021).
45. Ghatak, A., Brandenbourger, M., van Wezel, J. & Coulais, C. Observation of non-Hermitian topology and its bulk-edge correspondence in an active mechanical metamaterial. *Proc. Natl Acad. Sci.* **117**, 29561–29568 (2020).
46. Helbig, T. et al. Generalized bulk-boundary correspondence in non-Hermitian topolectrical circuits. *Nat. Phys.* **16**, 747–750 (2020).
47. Weidemann, S. et al. Topological funneling of light. *Science* **368**, 311–314 (2020).
48. Claes, J. & Hughes, T. L. Skin effect and winding number in disordered non-Hermitian systems. *Phys. Rev. B* **103**, L140201 (2021).
49. Longhi, S. Spectral deformations in non-Hermitian lattices with disorder and skin effect: A solvable model. *Phys. Rev. B* **103**, 144202 (2021).
50. Kim, K.-M. & Park, M. J. Disorder-driven phase transition in the second-order non-Hermitian skin effect. *Phys. Rev. B* **104**, L121101 (2021).
51. Gu, Z. et al. Transient non-Hermitian skin effect. *Nat. Commun.* **13**, 7668 (2022).
52. Wang, W., Wang, X. & Ma, G. Non-Hermitian morphing of topological modes. *Nature* **608**, 50 (2022).
53. Lee, E., Lee, H. & Yang, B.-J. Many-body approach to non-Hermitian physics in fermionic systems. *Phys. Rev. B* **101**, 121109 (2020).
54. Zhang, S.-B., Denner, M. M., Bzdušek, T., Sentef, M. A. & Neupert, T. Symmetry breaking and spectral structure of the interacting Hatano-Nelson model. *Phys. Rev. B* **106**, L121102 (2022).
55. Kawabata, K., Shiozaki, K. & Ryu, S. Many-body topology of non-Hermitian systems. *Phys. Rev. B* **105**, 165137 (2022).
56. Alsallom, F., Herviou, L., Yazyev, O. V. & Brzezińska, M. Fate of the non-Hermitian skin effect in many-body fermionic systems. *Phys. Rev. Res.* **4**, 033122 (2022).
57. Liu, T., He, J. J., Yoshida, T., Xiang, Z.-L. & Nori, F. Non-Hermitian topological Mott insulators in one-dimensional fermionic superlattices. *Phys. Rev. B* **102**, 235151 (2020).
58. Longhi, S. Spectral Structure and Doublon Dissociation in the Two-Particle Non-Hermitian Hubbard Model. *Ann. der Phys.* **535**, 2300291 (2023).
59. Mostafazadeh, A. Pseudo-Hermiticity versus PT-symmetry. II. A complete characterization of non-Hermitian Hamiltonians with a real spectrum. *J. Math. Phys.* **43**, 2814–2816 (2002).
60. Mostafazadeh, A. Pseudo-Hermiticity versus PT symmetry: The necessary condition for the reality of the spectrum of a non-Hermitian Hamiltonian. *J. Math. Phys.* **43**, 205–214 (2002).
61. Heußen, S., White, C. D. & Refael, G. Extracting many-body localization lengths with an imaginary vector potential. *Phys. Rev. B* **103**, 064201 (2021).
62. H. L. Essler, F., Frahm, H., Göhmann, F., Klümper, A. & E. Korepin, V. *The one-dimensional Hubbard model*. (Cambridge University Press, Cambridge, 2010).
63. Longhi, S. Topological Phase Transition in non-Hermitian Quasicrystals. *Phys. Rev. Lett.* **122**, 237601 (2019).
64. Longhi, S. Probing non-Hermitian skin effect and non-Bloch phase transitions. *Phys. Rev. Res.* **1**, 023013 (2019).
65. Haga, T., Nakagawa, M., Hamazaki, R. & Ueda, M. Liouvillian Skin Effect: Slowing Down of Relaxation Processes without Gap Closing. *Phys. Rev. Lett.* **127**, 070402 (2021).
66. Li, H., Wu, H., Zheng, W. & Yi, W. Many-body non-Hermitian skin effect under dynamic gauge coupling. *Phys. Rev. Res.* **5**, 033173 (2023).

Acknowledgements

We acknowledge Jung-Wan Ryu, Hee Chul Park, and Sonu Verma for fruitful discussion. This work was supported from the Institute for Basic Science in the Republic of Korea through the Project No. IBS-R024-D1. This work was supported by the National Research Foundation of Korea (NRF) grant funded by the Korea government (MSIT) (Grants No. RS-2023-00252085 and No. RS-2023-00218998).

Author contributions

B.H.K. performed the calculations of the work. B.H.K. and J.-H.H. constructed the main idea and the manuscript. B.H.K., J.-H.H., and M.J.P. contributed to the writing of the manuscript.

Competing interests

The authors declare no competing interests.

Additional information

Supplementary information The online version contains supplementary material available at https://doi.org/10.1038/s42005-024-01564-2.

Correspondence and requests for materials should be addressed to Moon Jip Park.

Peer review information *Communications Physics* thanks Stefano Longhi and the other, anonymous, reviewer(s) for their contribution to the peer review of this work. A peer review file is available.